ARPN Journal of Engineering and Applied Sciences

CLASSICAL AND PREDICTIVE CONTROL APPLIED TO A DC/DC SINGLE-ENDED PRIMARY INDUCTANCE CONVERTER

Andy D. Losada-Pacheco, Brayan C. Bravo-Fierro and Diego F. Sendoya-Losada
Department of Electronic Engineering, Faculty of Engineering, Surcolombiana University, Neiva, Huila, Colombia
E-Mail: diego.sendoya@usco.edu.co

ABSTRACT

In this work, two controllers, a Proportional Integral (PI) and a Model-based Predictive Controller (MPC), have been designed to regulate a DC/DC Single-Ended Primary Inductance Converter (SEPIC). First, the modeling and linearization of the system was performed using a frequency response estimation method. Then, the PI controller was designed around a certain setpoint. Next, an algorithm was designed according to the Extended Prediction Self-Adaptive Control (EPSAC). Finally, the performance of the controllers was evaluated for setpoint tracking and disturbance rejection.

Keywords: EPSAC, MPC, PI, RMSE, SEPIC.

1. INTRODUCTION

The DC/DC converter is an electrical circuit that transfers energy from a DC voltage source to a load. The energy is first transferred via electronic switches (transistors and diodes) to energy storage devices (inductors and capacitors) and then, subsequently switched from storage into the load. This process of energy transfer results in an output voltage that is related to the input voltage by the duty ratios of the switches.

DC/DC converters have applications in various areas such as Telecommunications, Industrial Robotics, Aerospace & Defense, Medical, Consumer and Automotive, among others. DC/DC converters are used in portable electronic devices such as mobile phones and laptops, which are mainly powered by batteries. Such electronic devices often contain multiple sub-circuits, each with its own voltage level requirement different from the one supplied by the battery or external source. For example, a lithium battery powers a laptop computer, and several DC/DC converters change the battery voltage into the voltages required by the loads. A buck converter produces the low-voltage DC required by the microprocessor. A boost converter increases the battery voltage to the level needed by the disk drive. In a power system, of an earth-orbiting spacecraft, a solar array produces the main power bus voltage. DC/DC converters convert bus voltage to the regulated voltages required by the spacecraft payloads. Battery charge/discharge controllers interface the main power bus to batteries; these controllers may also contain DC/DC converters.

Due to its importance and large number of application areas, the Alternative Energy Research Seedbed of the Surcolombiana University, is investigating various control techniques that allow obtaining a specific and regulated output voltage for various types of DC/DC converters. In the literature review, a large amount of information related to the analysis, design, and control of DC/DC converters can be found. In those studies, they have used classical and advanced techniques to control voltage, current or duty cycle, and, in this way, maintain a proper functioning of the circuit in different situations [1-11].

In this contribution, Model-based Predictive Control (MPC) is applied to a Single-Ended Primary Inductance Converter (SEPIC), in which a Single-Input Single-Output (SISO) system configuration has been considered. The circuit is powered with an input voltage of 9 V, the output voltage, V_o, is the controlled variable and the duty cycle, D, is the manipulated variable. Usually, the control of the linear systems is done by classical control techniques such as PI, due to its well-known and simple structure. For the design of these conventional controllers, it is necessary to choose a setpoint and then to find a linear model of the system, ensuring that the control works well in this region, but when it moves away from the setpoint, the controller loses effectiveness. In this contribution, the Extended Predictive Self-Adaptive Control (EPSAC) algorithm is used to setpoint tracking and disturbance rejection. Then, a comparison is made with the classic PI control to demonstrate the effectiveness of the proposed algorithm. The performance of these controllers is tested and evaluated in a simulation environment. Simulation is done using Matlab®/Simulink® software.

2. MATERIALS AND METHODS

2.1 Process Model

The circuit shown in Figure-1 is known as a SEPIC.

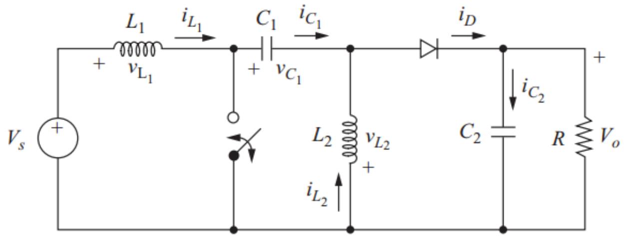

Figure-1. Schematic of SEPIC.

ARPN Journal of Engineering and Applied Sciences

The DC/DC SEPIC has the following parameters: $V_s = 9\,\text{V}$, $L_1 = 90\,\mu\text{H}$, $L_2 = 90\,\mu\text{H}$, $C_1 = 80\,\mu\text{F}$, $C_2 = 80\,\mu\text{F}$, $R = 3\,\Omega$. When the switching frequency $f = 100$ KHz and $D = 0.4$, the following open-loop response is obtained.

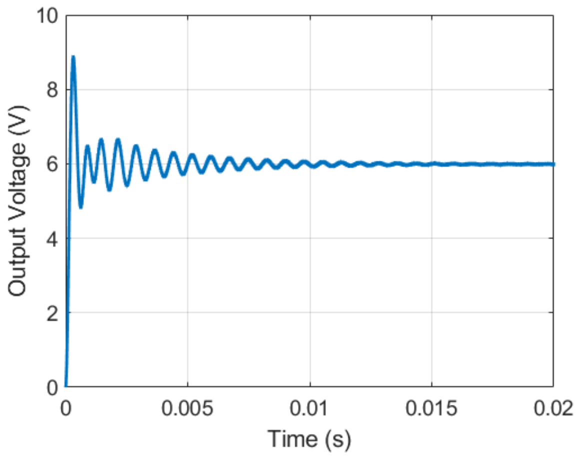

Figure-2. Open-loop response.

It can be seen that the output voltage has an overshoot $OS = 48.57\%$ and a settling time $t_s = 7.59$ ms. The steady-state output voltage is $V_o = 6$ V. Therefore, a controller is required to improve the performance of the closed-loop system. The design of the controller requires a mathematical representation of the circuit.

Analysis of the SEPIC begins by making these assumptions:

a) The circuit is operating in the steady-state, meaning that voltage and current waveforms are periodic.
b) Both inductors are very large and the currents in them are constant.
c) Both capacitors are very large and the voltages across them are constant.
d) The switching period is T; the switch is closed for time DT and open for time $(1-D)T$.
e) The components are ideal.

The inductor current and capacitor voltage restrictions will be removed later to investigate the fluctuations in currents and voltages. The inductor currents are assumed to be continuous in this analysis. Other observations are that the average inductor voltages are zero and that the average capacitor currents are zero for steady-state operation.

Kirchhoff's voltage law around the path containing V_s, L_1, C_1, and L_2 gives

$$-V_s + v_{L1} + v_{C1} - v_{L2} = 0 \tag{1}$$

Using the average of these voltages:

$$-V_s + 0 + V_{C1} - 0 = 0 \tag{2}$$

showing that the average voltage across the capacitor C_1 is

$$V_{C1} = V_s \tag{3}$$

When the switch is closed, the diode is off, and the voltage across L_1 for the interval DT is

$$v_{L1} = V_s \tag{4}$$

When the switch is open, the diode is on, and the Kirchhoff's voltage law around the outermost path gives

$$-V_s + v_{L1} + v_{C1} + V_o = 0 \tag{5}$$

Assuming that the voltage across C_1 remains constant at its average value of V_s (3):

$$-V_s + v_{L1} + V_s + V_o = 0 \tag{6}$$

$$v_{L1} = -V_o \tag{7}$$

for the interval $(1-D)T$. Since the average voltage across an inductor is zero for periodic operation, (4) and (7) are combined to get:

$$(v_{L1})_{\text{closed}} DT + (v_{L1})_{\text{open}}(1-D)T = 0 \tag{8}$$

$$V_s DT - V_o(1-D)T = 0 \tag{9}$$

Solving for V_o:

$$V_o = V_s\left(\frac{D}{1-D}\right) \tag{10}$$

This result shows that the variable to control depends on the duty cycle and the input voltage. The latter will be very useful to know the controller disturbance rejection. This result is similar to that of the buck-boost and Ćuk converter equations, with the important distinction that there is no polarity reversal between input and output voltages. The ability to have an output voltage greater or less than the input with no polarity reversal makes this converter suitable for many applications such as: output voltage corrector in lithium batteries, when the voltage is above or below that expected; in household appliances (washing machines, televisions) to raise the voltage after the rectification stage.

In order to obtain a mathematical model that represents the dynamics between V_o and D, a chirp signal is used to make the duty cycle vary sinusoidally with amplitude between 0.39 and 0.41, from a frequency of 30 Hz to 10 KHz. These changes originate an output voltage that also changes sinusoidally, which makes it possible to construct a Bode diagram (Figure-3) and, in this way, to estimate the transfer function between V_o and D.

ARPN Journal of Engineering and Applied Sciences

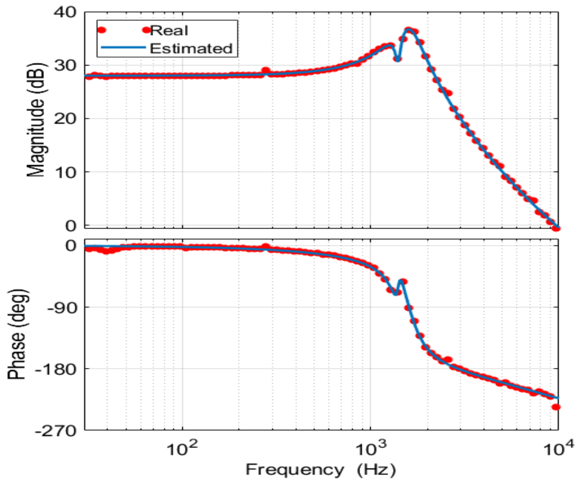

Figure-3. Bode plot for transfer function estimation.

This transfer function is a linear representation of the system when the setpoint is 6 V, with a fit to estimation data of 94.59%:

$$\frac{V_O(s)}{D(s)} = \frac{-4.262e04\, s^3 + 2.485e09\, s^2 - 1.873e12\, s + 1.94e17}{s^4 + 4584\, s^3 + 1.81e08\, s^2 + 3.807e11\, s + 7.722e15} \quad (11)$$

2.2 PI Controller Design

To improve the behavior of the closed-loop system, a PI controller is initially designed. The design criteria were that the controlled system output had the minimum settling time and overshoot, and that the PI controller output was between 0 and 1, which corresponds to the limits of the duty cycle.

The algorithm that describes the behavior of the PI controller is:

$$u(t) = K_p e(t) + K_i \int_0^t e\,(\tau) d\tau \quad (12)$$

$u(t)$ is the output signal of the PI controller, which in this case corresponds to the duty cycle. $e(t)$ is the input signal of the PI controller, which is defined as $e(t) = r(t) - y(t)$, where $r(t)$ is the setpoint and $y(t)$ is the output of the process, that is, the output voltage. K_p is the proportional gain and K_i is the integral gain [12-16].

Applying the Laplace transform, the transfer function of the PI controller is found:

$$\frac{U(s)}{E(s)} = K_p + \frac{K_i}{s} = 0.0017 + \frac{43.9552}{s} \quad (13)$$

2.3 EPSAC

It is common practice in MPC to structure the future control scenario. At each current moment t, the process output $y(t+k)$ is predicted over a time horizon $k = 1 \dots N_2$. The predicted values are indicated by $y(t+k|t)$ and the value N_2 is called the prediction horizon. A prediction horizon $N_2 = 12$ is used in this work. The prediction model used is given in (11). The forecast depends on the past inputs and outputs, but also on the future control scenario $u(t+k|t)$ with $k = 0 \dots N_2 - 1$. This can be done by defining a control horizon N_u with $1 \le N_u \le N_2$, after which the control strategy remains constant, i.e. $u(t+k|t) = u(t+N_u-1|t)$ for $N_u \le k \le N_2 - 1$ [17].

Conceptually the future response $y(t+k|t)$ can be considered as the cumulative result of 2 effects: $y_{\text{base}}(t+k|t)$, which is calculated based on the effect of future disturbances $n(t+k|t)$, the effect of past control $u(t-1)$, $u(t-2)$, … and the effect of a basic future control scenario $u_{\text{base}}(t+k|t)$ with $k = 0 \dots N_2 - 1$; and $y_{\text{opt}}(t+k|t)$, which is the effect of the optimizing future control actions $\delta u(t+k|t)$ with $k = 0 \dots N_2 - 1$, i.e. $\delta u(t+k|t) = u(t+k|t) - u_{\text{base}}(t+k|t)$, where $u(t+k|t)$ is the optimal control input that is sought [18].

Structuring leads to simplified calculations by reducing the degrees of freedom of the control vector from N_2 to N_u and generally has a positive effect on robustness. The extremely simplified version $N_u = 1$ leads to remarkably good results in many practical applications [19]. Hence, a control horizon $N_u = 1$ is used in this work. The control horizon implies that $u_{\text{base}}(t+k|t) = u_{\text{base}}(t|t)$ and $\delta u(t+k|t) = \delta u(t|t)$ for $1 \le k \le N_2 - 1$. Furthermore, $y_{\text{opt}}(t+k|t)$ —being the result of $\delta u(t+k|t)$- is the effect of a single step input with amplitude $\delta u(t|t)$ at time t. The system output at time $t+k$ is thus, $y_{\text{opt}}(t+k|t) = g_k \delta u(t|t)$ for $1 \le k \le N_2$, where g_k for $k = 1 \dots N_2$ are the coefficients of the unit step response of the system [20].

For a linear system with constant parameters, the step response coefficients are constant and thus must be calculated only once. Using matrix notation, $Y_{\text{opt}} = GU$:

$$\begin{bmatrix} y_{opt}(t+1|t) \\ y_{opt}(t+2|t) \\ \dots \\ y_{opt}(t+N_2|t) \end{bmatrix} = \begin{bmatrix} g_1 \\ g_2 \\ \dots \\ g_{N_2} \end{bmatrix} \delta u(t|t) \quad (14)$$

The key EPSAC equation is then $Y = Y_{\text{base}} + Y_{\text{opt}}$. The task of the controller is to find the control vector $u(t+k|t)$ with $k = 0 \dots N_2 - 1$ that minimizes the cost function:

$$\sum_{k=N_1}^{N_2} [r(t+k|t) - y(t+k|t)]^2 = (R-Y)^T (R-Y) \quad (15)$$

where the default value for N_1 is the systems time delay, $N_1 = 1$ is used in this work. $r(t+k|t)$ is the reference trajectory, which is in this case the setpoint R. Minimization of (15) with respect to U gives the optimal solution:

$$U^* = (G^T G)^{-1} G^T (R - Y_{\text{base}}) \quad (16)$$

ARPN Journal of Engineering and Applied Sciences

Since the control horizon is chosen $N_u = 1$, the matrix $G^T G$ with dimensions $N_u \times N_u$ is a scalar and thus its inversion has a low computational cost. The actual control action applied to the real process at the current time t is $u(t) = u_{\text{base}}(t|t) + \delta u(t|t)$, i.e.:

$$u(t) = u_{\text{base}}(t|t) + U^*(1) \tag{17}$$

At the next sampling instant $t+1$, the whole procedure is repeated by considering the new measurement information $y(t+1)$ (so-called receding horizon) [21].

Clipping is applied to the control action whenever necessary because the limits of the duty cycle are between 0 and 1.

3. RESULTS AND DISCUSSIONS

The simulation was conducted towards two scenarios to compare the behavior of the PI and EPSAC algorithms. The performance of the controllers is evaluated, in order to carry out a tracking to a reference voltage and an effective rejection of the disturbances.

3.1 Scenario 1: Disturbance Rejection

In order to evaluate the performance of the controlled system when a disturbance is applied, the voltage reference or setpoint is fixed at 6 V.

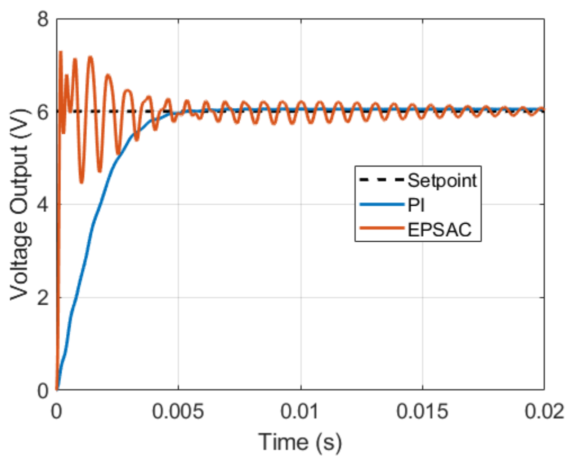

Figure-4. Closed-loop response.

It can be seen that when the PI controller is used, the closed-loop response presents no overshoot ($OS = 0\%$), and the settling time decreases with respect to the open-loop response ($t_s = 4.39$ ms). On the other hand, when the EPSAC algorithm is used, the response presents a lower overshoot and a settling time higher than those observed in open-loop ($OS = 21.67\%$ and $t_s = 16.13$ ms). Even the steady-state response exhibits small oscillations around the setpoint.

Figure-5 shows the control actions developed by each controller. Initially, the control effort of the EPSAC algorithm is greater than that of the PI controller, which explains the higher response speed in closed-loop. As steady-state is reached, the two controllers deliver the same duty cycle ($D = 0.4$).

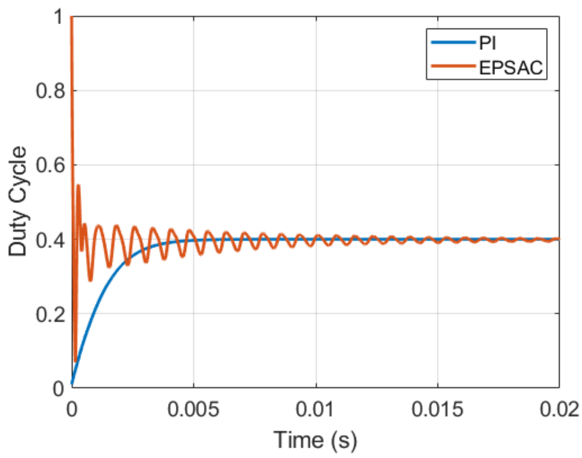

Figure-5. Duty cycle with PI and EPSAC algorithms.

After the response reaches the steady-state a disturbance is applied to the system, which consists of a change in the input voltage, that is, V_s goes from 9 V to 10 V at 20 ms. Finally, when the response reaches the steady-state again, the input voltage is changed from 10 V to 8 V at 40 ms. Figure-6 shows the output voltage when PI and EPSAC (prediction horizon $N_2 = 12$) algorithms are used. This prediction horizon is used because it allows the response to have the shortest settling time with a small overshoot.

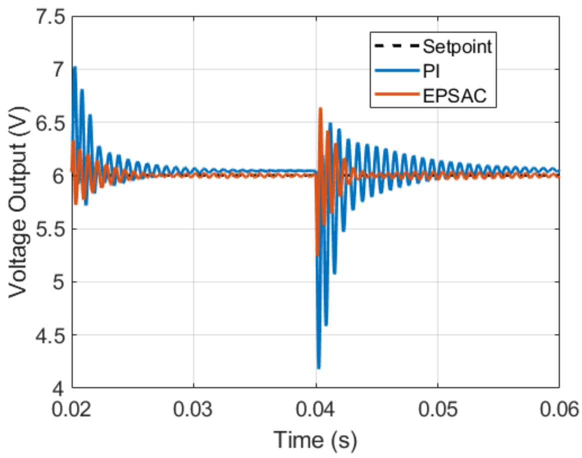

Figure-6. Disturbance rejection.

It can be seen that when the PI controller is used, the rejection of the disturbance is not very effective, since the steady-state is achieved 5.49 ms after the first disturbance is applied, and 11.1 ms after the second disturbance is applied. Furthermore, the response presents a small steady-state error in both cases. On the other hand, when the EPSAC algorithm is used, the steady-state is

ISSN 1819-6608
ARPN Journal of Engineering and Applied Sciences

achieved 2.17 ms after the first disturbance is applied, and 2.43 ms after the second disturbance is applied.

Figure-7 shows that when the first disturbance is applied at 20 ms, both algorithms reduce the duty cycle from 0.4 to 0.37. However, the output of the EPSAC algorithm has more oscillations. When the second disturbance is applied at 40 ms, both algorithms increase the duty cycle from 0.37 to 0.43. Again, oscillations in the output of the EPSAC algorithm are observed.

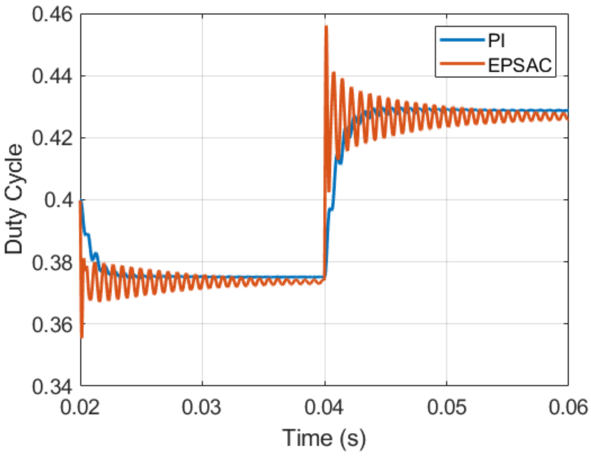

Figure-7. Duty cycle for disturbance rejection with PI and EPSAC algorithms.

3.2 Scenario 2: Setpoint Tracking

In order to evaluate how the system behaves in closed-loop at different setpoints, a voltage reference signal composed of 3 steps with amplitudes of 6 V, 7 V, and 5 V is applied. Figure-8 shows how the process output $y(t)$ tracks a setpoint for a prediction horizon $N_2 = 12$.

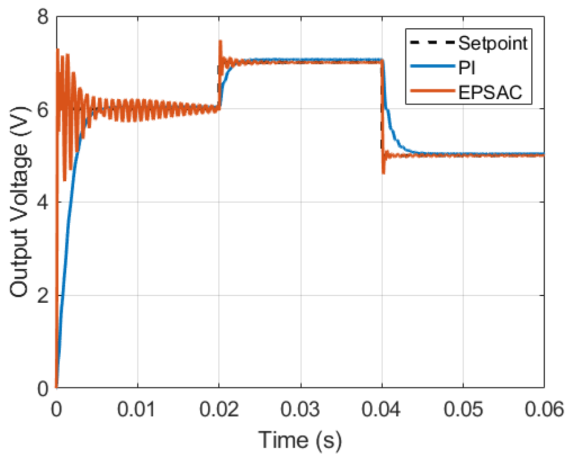

Figure-8. Setpoint tracking.

For the reference voltage of 6 V, it can be seen that, when the PI controller is used, the closed-loop response presents no overshoot ($OS = 0\%$), and the settling time decreases with respect to the open-loop response ($t_s = 4.39$ ms). On the other hand, when the EPSAC algorithm is used, the response presents a lower overshoot and a settling time higher than those observed in open-loop ($OS = 21.67\%$ and $t_s = 16.13$ ms). Even the steady-state response exhibits small oscillations around the setpoint. At 20 ms, when the reference voltage is increased to 7 V, it can be seen that the closed-loop response, when the PI controller is used, presents the same overshoot ($OS = 0\%$), but the settling time is lower ($t_s = 1.4$ ms). On the other hand, when the EPSAC algorithm is used, the response presents a small overshoot and a settling time lower than those observed in open-loop ($OS = 6.84\%$ and $t_s = 0.4$ ms). Finally, at 40 ms, when the reference voltage decreases to 5 V, it can be seen that the closed-loop response, when the PI controller is used, does not have a negative undershoot ($US = 0\%$), but the settling time is higher ($t_s = 3.43$ ms). On the other hand, when the EPSAC algorithm is used, the response has a larger negative undershoot and settling time ($US = 7.96\%$ and $t_s = 0.66$ ms).

Figure-9 shows the control actions performed by each controller. Initially, the control effort of the EPSAC algorithm is greater than that of the PI controller, which explains the higher response speed in closed-loop. As steady-state is reached, the two controllers deliver the same duty cycle ($D = 0.4$). At 20 ms, both algorithms increase the duty cycle from 0.4 to 0.44, however the output of the EPSAC algorithm shows more oscillations. At 40 ms, both algorithms reduce the duty cycle from 0.44 to 0.35. In all cases, it can be seen that the variations in the duty cycle originated by the EPSAC algorithm are more pronounced than those of the PI controller, which allows faster changes in the output voltage.

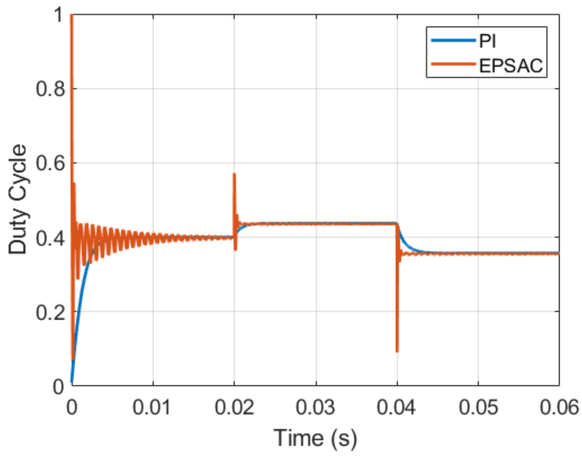

Figure-9. Duty cycle for setpoint tracking with PI and EPSAC algorithms.

3.3 RMSE

In order to obtain a detailed results analysis of the comparative study between the PI and EPSAC algorithms, the Root Mean Square Error (RMSE) variations were used. RMSE measures the amount of error between two data sets:

ISSN 1819-6608
ARPN Journal of Engineering and Applied Sciences

$$RMSE = \sqrt{\frac{\sum_{t=1}^{N}[r(t)-y(t)]^2}{N}} \qquad (18)$$

where $r(t)$ is the setpoint signal, $y(t)$ is the output signal, and N is the number of samples. Figure-10 shows that the quality of the response is much better when the EPSAC algorithm is used.

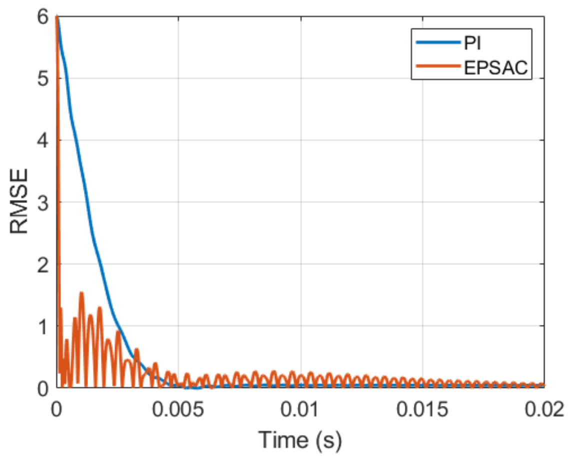

Figure-10. RMSE variations for PI and EPSAC algorithms.

Table-1 shows the RMSE variations for both the PI controller and the EPSAC algorithm when the two simulation scenarios are applied.

Table-1. RMSE Variations for PI and EPSAC.

Scenario	PI (%)	EPSAC (%)
1	3.11	0.11
2	8.95	0.70

The implemented EPSAC algorithm presents a better behavior in the two scenarios compared to the PI algorithm.

Although the computational cost of the implementation of the EPSAC algorithm is higher, the system response is noticeably faster than when the PI controller is used. This can be an advantage in systems where it is necessary to minimize the values of overshoot and settling time. However, for processes where these requirements are not necessary, the PI algorithm would be more viable because of its simplicity of implementation.

4. CONCLUSIONS

In this work, the performance of PI and EPSAC algorithms was evaluated. It can be observed that the EPSAC is more effective in rejecting disturbances. This is because changes in the duty cycle are more pronounced when there are changes in the input voltage. In the same way, because the EPSAC uses the linear model of the plant to make the predictions, then the tracking to the variations in the reference voltage is much better. In addition, the control effort required is greater when changing from one setpoint to another.

REFERENCES

[1] Zhu Y. and W. Xiao. 2020. A comprehensive review of topologies for photovoltaic I-V curve tracer. Solar Energy. 196: 346-357.

[2] Rehman Zubair, Ibrahim Al-Bahadly and Subhas Mukhopadhyay. 2015. Multiinput DC-DC converters in renewable energy applications-An overview. Renewable and Sustainable Energy Reviews. 41: 521-539.

[3] Sivakumar S., et al. 2016. An assessment on performance of DC-DC converters for renewable energy applications. Renewable and Sustainable Energy Reviews. 58: 1475-1485.

[4] Khosrogorji S., et al. 2016. Multi-input DC/DC converters in connection with distributed generation units-A review. Renewable and sustainable energy reviews. 66: 360-379.

[5] Zhang, Neng, Danny Sutanto and Kashem M. Muttaqi. 2016. A review of topologies of three-port DC-DC converters for the integration of renewable energy and energy storage system. Renewable and Sustainable Energy Reviews. 56: 388-401.

[6] Revathi, B. Sri, and M. Prabhakar. 2016. Non isolated high gain DC-DC converter topologies for PV applications-A comprehensive review. Renewable and Sustainable Energy Reviews. 66: 920-933.

[7] Arunkumari T. and V. Indragandhi. 2017. An overview of high voltage conversion ratio DC-DC converter configurations used in DC micro-grid architectures. Renewable and Sustainable Energy Reviews. 77: 670-687.

[8] Singh S. N. 2017. Selection of non-isolated DC-DC converters for solar photovoltaic system. Renewable and Sustainable Energy Reviews. 76: 1230-1247.

[9] Gopi, R. Reshma and S. Sreejith. 2018. Converter topologies in photovoltaic applications- A review. Renewable and Sustainable Energy Reviews. 94: 1-14.

[10] Hossain M. Z. and N. A. Rahim. 2108. Recent progress and development on power DC-DC

VOL. 16, NO. 12, JUNE 2021 ISSN 1819-6608
ARPN Journal of Engineering and Applied Sciences

www.arpnjournals.com

converter topology, control, design and applications: A review. Renewable and Sustainable Energy Reviews. 81: 205-230.

[11] Amir Asim, et al. 2019. Comparative analysis of high voltage gain DC-DC converter topologies for photovoltaic systems. Renewable energy. 136: 1147-1163.

[12] Sendoya-Losada Diego F., Vargas-Duque Diana C., and Ávila-Plazas Ingrid J. 2018. Implementation of a neural control system based on PI control for a non-linear process. 2018 IEEE 1st Colombian Conference on Applications in Computational Intelligence (ColCACI). IEEE.

[13] Sendoya-Losada, Diego F. and Quintero-Polanco, Jesús D. 2108. Control of yaw angle in a miniature helicopter. ARPN Journal of Engineering and Applied Sciences. 13: 620-626.

[14] Sendoya-Losada, Diego F., and Quinterro-Polanco, Jesús D. 2018. PID controller applied to an unmanned aerial vehicle. ARPN Journal of Engineering and Applied Sciences. 13: 325-334.

[15] Sendoya-Losada Diego F. and Quintero-Polanco Jesús D. 2018. Design and validation of a pid auto-tuning algorithm. ARPN Journal of Engineering and Applied Sciences. 13: 3797-3802.

[16] Sendoya-Losada Diego F. 2108. KCR PID auto-tuner algorithm applied to a FOT device. ARPN Journal of Engineering and Applied Sciences. 13: 2505-2510.

[17] Sendoya-Losada D. F. 2109. Principles, applications and perspectives of predictive control. ARPN Journal of Engineering and Applied Sciences. 14: 2464-2467.

[18] Sendoya-Losada, D.F., Robayo Betancourt, Faiber, and Salgado Patrón José. 2107. Application of a predictive controller with variable time delay ingeneral anesthesia. ARPN Journal of Engineering and Applied Sciences. 12: 2661-2667.

[19] Sendoya-Losada Diego F. and Molina Mosquera, Johan J. 2107. Linear and nonlinear predictive control algorithms applied to a heated tank system. ARPN Journal of Engineering and Applied Sciences. 12: 6895-6903.

[20] Sendoya-Losada Diego F., Arroyave-Quezada José O. and Velasquez-Pobre Alvaro J. 2109. EPSAC and NEPSAC algorithms applied to a non-linear liquid level system. 2019 IEEE 4th Colombian Conference on Automatic Control (CCAC). IEEE.

[21] Pulido-Cortes German A., Moreno-Artunduaga, Alejandro and Sendoya-Losada Diego F. 2020. Classical and predictive control applied to a non-linear system of coupled tanks. ARPN Journal of Engineering and Applied Sciences. 15: 1466-1471.